

THE ACCELERATION OF ELECTRONS AT COLLISIONLESS SHOCKS MOVING THROUGH A TURBULENT MAGNETIC FIELD

FAN GUO¹ AND JOE GIACALONE²

Draft version February 2, 2015

ABSTRACT

We perform a numerical-simulation study of the acceleration of electrons at shocks that propagate through a prespecified, kinematically defined turbulent magnetic field. The turbulence consists of broadband magnetic fluctuations that are embedded in the plasma and cover a range of wavelengths, the smallest of which is larger than the gyroradii of electrons that are initially injected into the system. We find that when the variance of the turbulent component of the upstream magnetic field is sufficiently large – $\sigma^2 \sim 10 B_0^2$, where B_0 is the strength of the background magnetic field – electrons can be efficiently accelerated at a collisionless shock regardless of the orientation of the mean upstream magnetic field relative to the shock-normal direction. Since the local angle between the incident magnetic-field vector and the shock-normal vector can be quite large, electrons can be accelerated through shock-drift acceleration at the shock front. In the upstream region, electrons are mirrored back to the shock front leading to multiple shock encounters. Eventually the accelerated electrons are energetic enough that their gyroradii are of the same order as the wavelength of waves that are included in our description of the turbulent magnetic field. Our results are consistent with recent *in situ* observations at Saturn’s bow shock. The study may help understand the acceleration of electrons at shocks in space and astrophysical systems.

Subject headings: acceleration of particles - cosmic rays - shock waves - turbulence

1. INTRODUCTION

Collisionless shocks in space and other astrophysical systems have been observed to be strong sources of energetic charged particles (Blandford & Eichler 1987). Diffusive shock acceleration (DSA; Krymsky 1977; Axford et al. 1977; Bell 1978; Blandford & Ostriker 1978) is the primary theory that describes quantitatively the acceleration process in the vicinity of shock waves. The process is expected to occur in many places such as propagating interplanetary shocks, planetary bow shocks, the solar wind termination shock, supernova blast waves, and shocks driven by jets from active galactic nuclei. The theory of DSA works regardless the angle between the incident magnetic-field vector and the shock-normal vector θ_{Bn} , although the angle can greatly influence the acceleration of charged particles (Jokipii 1982, 1987). Most attention so far has been focused on the acceleration of ions. When the speeds of ions are large enough (usually a few times of the shock speed), they can interact resonantly with ambient magnetic turbulence and/or ion-scale waves and therefore get accelerated through DSA.

The acceleration of electrons at collisionless shock waves is more poorly understood than that of ions. For low-energy electrons, their gyroradii are too small for them to resonantly interact with pre-existing magnetic fluctuations or ion-generated waves in the shock region. The acceleration and scattering of low-rigidity particles, especially electrons, is thought to be difficult. This is usually referred to as the injection problem. For highly-

relativistic electrons, their gyroradii are close to gyroradii of ions at the same energy so that the acceleration of high-energy electrons by DSA is not a problem.

Electron acceleration at quasi-perpendicular shocks ($45^\circ < \theta_{Bn} < 90^\circ$) has been considered by a number of authors (Wu 1984; Krauss-Varban et al. 1989; Burgess 2006; Guo & Giacalone 2010, 2012a,b). Analytical theories and numerical simulations have shown that at quasi-perpendicular shocks, electrons can be accelerated through shock-drift acceleration (Wu 1984; Krauss-Varban et al. 1989; Yuan et al. 2008; Park et al. 2012). In this mechanism, charged particles drift because of the gradient in the magnetic field at the shock front. During the drift motion electrons gain energy along the motional electric field $\mathbf{E} = -\mathbf{V} \times \mathbf{B}/c$. However, it has been shown that in the scatter-free limit, the maximum attainable energy and the fraction of particles that gain a significant amount of energy are very limited at a planar shock (e.g., Ball & Melrose 2001). Recent numerical simulations have shown that non-planar effects such as small-scale ripples and magnetic fluctuations can greatly enhance the acceleration of electrons (Burgess 2006; Umeda et al. 2009; Guo & Giacalone 2010, 2012a; Yang et al. 2012). Whistler waves may play an important role during the acceleration process. Observational evidence of whistler waves for the acceleration of electrons at quasi-perpendicular shocks has been presented (Shimada et al. 1999; Oka et al. 2006; Wilson et al. 2012). However, the exact generation mechanism is under debate (Wu et al. 1983; Krasnoselskikh et al. 2002; Matsukiyo & Scholer 2006; Hellinger et al. 2007) and full particle-in-cell (PIC) simulations performed on this subject are limited to use an unrealistic set of parameters including the mass ratio m_i/m_e and the ratio between Alfvén speed and the speed of light v_A/c . For the cases with high Alfvén Mach

guofan.ustc@gmail.com

¹ Theoretical Division, Los Alamos National Laboratory, Los Alamos, NM 87545

² Department of Planetary Sciences and Lunar and Planetary Laboratory, University of Arizona, 1629 E. University Blvd., Tucson, AZ 85721

numbers and unrealistic mass ratios, some PIC simulations show that electrons can be efficiently accelerated in the electric field due to the Buneman instability excited at the shock foot (Shimada & Hoshino 2000; Hoshino & Shimada 2002; Amano & Hoshino 2007). However, whether this mechanism is robust for the realistic mass ratio $m_i/m_e = 1836$ in a proton-electron plasma and three-dimensional simulations is not clear (see Riquelme & Spitkovsky 2011).

The acceleration of electrons at the quasi-parallel shocks ($0^\circ < \theta_{Bn} < 45^\circ$) has been less understood. The role of whistler waves generated at quasi-parallel geometry has been considered by several authors (Levinson 1992, 1994; Amano & Hoshino 2010). In this mechanism, the thermal or shock-reflected electrons can generate whistler waves which in turn scatter electrons in pitch-angle. This mechanism requires a high Mach number in order for the efficient generation of whistler waves (Levinson 1992; Amano & Hoshino 2010). Significant electron acceleration has not been found in recent PIC simulations for collisionless shocks with high mach numbers (Kato & Takabe 2010; Riquelme & Spitkovsky 2011; Niemiec et al. 2012). Therefore it is not clear how electrons get efficient nonthermal acceleration at quasi-parallel shocks.

Effects of large-scale magnetic fluctuations have been shown to be important for accelerating both ions and electrons at shocks (Giacalone & Jokipii 1996; Giacalone 2005a,b; Jokipii & Giacalone 2007; Guo & Giacalone 2010, 2012a,b). Numerical simulations that consider large-scale pre-existing magnetic turbulence suggest the acceleration of low-rigidity particles is efficient and there is *no* injection problem (Giacalone 2005a,b). Using self-consistent hybrid simulations (kinetic ions and fluid electrons) combined with test-particle simulations for electrons, Guo & Giacalone (2010) have found efficient electron acceleration at perpendicular shocks moving through a plasma containing large-scale pre-existing magnetic turbulence. The turbulent magnetic field leads to field-line meandering that allows the electrons to get accelerated at the shock front multiple times. Small-scale shock ripples can also play a role in scattering electrons in pitch angles similar to what is shown by Burgess (2006). In a more recent paper, Guo & Giacalone (2012a) demonstrated that perpendicular shocks – which exist in some flare models – can efficiently accelerate both electrons and ions.

In previous works, wave variances of magnetic turbulence are usually taken to be $\sigma^2 \leq B_0^2$ (B_0 is the background magnetic field), consistent with typical values of the variance in the interplanetary magnetic field observed *in situ* by spacecraft. The acceleration of electrons is found to prefer perpendicular shocks and there is no significant acceleration at quasi-parallel shocks. It should be noted that when there are large-amplitude ambient magnetic fluctuations or ion-generated waves in the upstream region, locally the shock angle θ_{Bn} can get quite large even when the shock geometry is quasi-parallel, on average, and particles undergo acceleration by drifting along the shock due to the compressed transverse components of the magnetic field, as in shock-drift acceleration (Guo & Giacalone 2013).

In situ observations in the heliosphere have extensive evidence of energetic electrons associated with collision-

less shocks (e.g., Fan et al. 1964; Anderson et al. 1979; Gosling et al. 1989; Simnett et al. 2005; Decker et al. 2005). Examples include interplanetary shocks, planetary bow shocks, and the solar wind termination shock. These studies commonly found that electrons are accelerated at quasi-perpendicular shocks and there are rarely accelerated electrons at quasi-parallel shocks, suggesting that for those shocks, significant electron acceleration can only occur in quasi-perpendicular regions. Remote imaging and radio observations inferred that electrons are accelerated at quasi-perpendicular regions of coronal shocks (Kozarev et al. 2011; Feng et al. 2012, 2013). This indicates that for solar energetic particle (SEP) events, where the energetic electrons are observed to have tight correlations with energetic ions, quasi-perpendicular shocks may accelerate most energetic particles (Haggerty & Roelof 2009; Cliver 2009; Guo & Giacalone 2012b). However, in astrophysical shocks such as supernova blast waves, observations suggest that electrons can be accelerated to highly relativistic energy regardless of the shock angle, θ_{Bn} , although the local shock angle is not directly observable, and, therefore is not known (Reynolds 2008). For example, Chandra’s observations for Tycho supernova remnant have revealed strong non-thermal X-ray emissions surrounding the remnant, presumably caused by synchrotron radiations of strongly accelerated electrons in the shock region (e.g., Eriksen et al. 2011).

Recently, Masters et al. (2013) reported a rare *in situ* measurement where electrons can be accelerated to $\sim MeV$ in the quasi-parallel part of Saturn’s bow shock. The shock is observed to be associated with large-amplitude magnetic fluctuations ($\delta B/B_0 \sim 10$ or even larger). This indicates electrons can be efficiently accelerated at quasi-parallel shocks when large-amplitude magnetic fluctuations are present in the shock region.

In this paper, we explore the effect of strong large-scale magnetic fluctuations on the acceleration of electrons at collisionless shocks. We show electrons can be efficiently accelerated to high energy regardless of the angle between the average magnetic field and shock normal when strong large-scale magnetic fluctuations exist in the shock region ($\sigma^2 \sim 10B_0^2$). This finding can help understand the acceleration of electrons at astrophysical shocks such as recent *in situ* observation at Saturn’s bow shock (Masters et al. 2013) and radio and X-ray observations for supernova shocks (Reynolds 2008).

2. NUMERICAL METHOD

We integrate numerically the equations of motion of an ensemble of electrons in pre-specified, kinematically defined electric and magnetic fields in the shock region. This method resolves the gyromotions of charged particles close to the shock that is critical to the acceleration of low-rigidity particles. The electrons are assumed to have a negligible effect on the shock fields; thus, they are treated as test particles. The approach is similar to previous studies (Decker & Vlahos 1986; Decker 1988; Giacalone & Jokipii 1996; Giacalone 2005a) and we use it for electrons as was done by Giacalone & Jokipii (2009). Here we describe the salient details of the numerical method for completeness, the readers are referred to the previous papers for further details.

In the simulation, a planar shock is located at $x = 0$,

and plasma flows from $x < 0$ (upstream) with a speed of U_1 to $x > 0$ (downstream) with a speed of $U_2 = U_1/r$, where r is the compression ratio. The flow speed along the x direction is assumed to be

$$U(x) = \frac{2U_1}{(r+1) + (r-1)\tanh(x/\delta_{sh})}, \quad (1)$$

where δ_{sh} is the width of the shock. The upstream speed in the shock frame is taken to be $U_1 = 500$ km/s. Close to the shock, the flow speed varies smoothly across a sharp layer with $\delta_{sh} = 0.2U_1/\Omega_i$, where Ω_i is the upstream proton cyclotron frequency. This is similar to the observed high-Mach-number shocks (Bale et al. 2003). We assume a compression ratio for the strong shock limit $r = U_1/U_2 = 4$, corresponding to the case where both the upstream Alfvénic Mach number M_A and sonic Mach number M_s are much larger than 1. The dynamical evolution of the shock surface caused by the convection of magnetic fluctuations across the shock is neglected since the dynamical pressure is much larger than the magnetic pressure.

The magnetic field embedded in the plasma flow is given by the solution to the magnetic induction equation. In our model, the magnetic-field components are given by the convected magnetic field

$$\begin{aligned} B_x(x, y, z, t) &= B_x(x_0, y, z, t_0), \\ B_y(x, y, z, t) &= B_y(x_0, y, z, t_0) \left(\frac{U(x_0)}{U(x)} \right), \\ B_z(x, y, z, t) &= B_z(x_0, y, z, t_0) \left(\frac{U(x_0)}{U(x)} \right), \end{aligned} \quad (2)$$

where x_0 and t_0 can be related using the equation $dx/dt = U(x)$. Note that the transverse components of magnetic fields increase when the plasma is compressed. The solution to the equation can be expressed as

$$t - t_0 = \int_{x_0}^x \frac{dx'}{U(x')}. \quad (3)$$

We choose x_0 to be far upstream of the shock, and use Equation (3) to determine t_0 using the speed of plasma flow given in Equation (1). Using these values in Equation (2), the magnetic field vector is defined at any point in space and time as long as it is known at (x_0, y, z, t_0) . The field at this point is taken to be $\mathbf{B}(x_0, y, z, t_0) = \mathbf{B}_0(x_0) + \delta\mathbf{B}(x_0, y, z, t_0)$, where \mathbf{B}_0 is the average magnetic field lying in the x - z plane and $\delta\mathbf{B}$ is a random magnetic field component. For the fluctuation component, we assume purely isotropic magnetic fluctuations (Batchelor 1953), which is approximated by a large number of wave modes having wavevectors randomly distributed in direction and with random phases and polarizations. The amplitude of each mode is determined from an assumed Kolmogorov-like power spectrum. For more details on generating the turbulent magnetic fields, see Giacalone & Jokipii (1999). In our simulations, the correlation length is taken to be $L_c = 50U_1/\Omega_i$. The maximum and minimum wavelengths used to generate the turbulence are $\lambda_{max} = 500U_1/\Omega_i$ and $\lambda_{min} = 5U_1/\Omega_i$, respectively. Under typical conditions near Saturn's bow shock, the coherence length corresponds to a spatial scale of $\sim 10^5$ km. The motional electric field is obtained under the ideal MHD approximation $\mathbf{E} = -\mathbf{U} \times \mathbf{B}/c$. It

is important to note that our simulations utilize a fully three-dimensional magnetic field. This is essential for correctly considering cross-field diffusion as noted by previous works (Jokipii et al. 1993; Giacalone & Jokipii 1994; Jones et al. 1998).

In the simulation the electrons are injected upstream of the shock at a constant rate. This is done by initializing electrons immediately upstream ($x = -5U_1/\Omega_i$) with a time randomly chosen between $t = 0$ and t_{max} . The initial velocity distribution is isotropic in the local plasma frame with an energy of 1 keV. The relativistic equations of motion

$$\frac{d\mathbf{p}}{dt} = e(\mathbf{E} + \mathbf{v} \times \mathbf{B}), \quad (4)$$

$$\frac{d\mathbf{x}}{dt} = \mathbf{v}, \quad (5)$$

for each particle are numerically integrated using the Burlirsh-Stoer method (Press et al. 1986). The algorithm uses an adjustable time step based on an evaluation of the local truncation error. It is highly accurate and fast when fields are smooth compared with the electron gyroradius. The energy is conserved to an accuracy of better than 0.1% of the total energy in the plasma frame when the shock is not considered in our simulation. For the parameters we use, the initial gyroradii of electrons are about $0.02U_1/\Omega_i$, much less than the thickness of the shock layer and the spatial scale of the injected magnetic fluctuations. In the end of the simulations, the maximum energy of electrons reaches energies exceeding an MeV and their gyroradii become large enough for them to interact resonantly with the injected magnetic fluctuations. No spatial boundary is placed in the simulation. We numerically integrate the trajectory of about 5 million test particles for each case. The trajectories for all the electrons are integrated until $\Omega_i t_{max} = 400.0$. At the end of the simulation, some accelerated electrons can propagate to a distance of several thousand U_1/Ω_i away from the shock. The electrons considered in this work are tracked in a much larger spatial region than that is achievable in recent two- and three-dimensional particle-in-cell simulations (Giacalone & Ellison 2000; Guo & Giacalone 2010, 2013; Caprioli & Spitkovsky 2013). We vary the turbulence variance, σ^2 , and angle between the average magnetic field and shock normal, θ_{Bn} , in our calculations in order to understand their effect on the energization of electrons, and particularly on the energy spectrum. We also calculate the fraction of electrons with energies $E > 10$ keV at the end of the simulation. This is used to characterize the efficiency of electron acceleration. Table 1 lists the parameters for each run.

We assume that the electrons have a negligible effect on the electric and magnetic fields close to the shock. We also neglect shock microstructure such as magnetic overshoot, and cross-field electric field, etc. Note that those effects modify the motion of a single particle at the shock front, but do not change the main conclusion of the current study. For example, considering magnetic overshoot can increase the population of electrons that gain energy through adiabatic reflection (Wu 1984). The cross-shock potential is much less than the initial electron energy per charge, meaning ignoring that effect does not significantly change the results.

Run	$\sigma^2(B_0^2)$	θ_{Bn}	$\Gamma\%(E > 10\text{keV})$
1	0.1	0	0.0
2	0.1	15	0.0
3	0.1	30	0.0
4	0.1	45	0.0
5	0.1	60	0.2
6	0.1	75	0.97
7	0.1	90	9.3
8	1.0	0	1.8
9	1.0	15	2.1
10	1.0	30	2.58
11	1.0	45	3.78
12	1.0	60	6.04
13	1.0	75	9.5
14	1.0	90	13.5
15	10	0	7.3
16	10	15	7.5
17	10	30	7.9
18	10	45	8.6
19	10	60	9.7
20	10	75	10.9
21	10	90	11.4

TABLE 1

PARAMETERS FOR EACH SIMULATION RUN. THE TOTAL WAVE VARIANCE $\delta B^2/B_0^2$. THE AVERAGED SHOCK NORMAL ANGLE θ_{Bn} , AND THE FRACTION OF ELECTRONS WHOSE ENERGY IS MORE THAN 10 keV AT THE END OF SIMULATION.

3. SIMULATION RESULTS

Using numerical simulations described in Section 2, we examine the effects of wave variances σ^2 and average shock angles θ_{Bn} on the acceleration of electrons at shocks. Table 1 lists the parameters for each run. It also contains the fraction of electrons with energies $E > 10$ keV at the end of the simulation for each simulation run. This is used to characterize the efficiency of electron acceleration.

Figure 1 shows the magnetic field magnitude along the x direction in the upper panel. In this case (Run 16), the average shock angle $\theta_{Bn} = 15^\circ$ and the wave variance of magnetic fluctuations $\sigma^2 = 10B_0^2$. The upstream magnetic field is featured by large-amplitude magnetic fluctuations. The magnitude of the magnetic-field increases at the shock due to the compression of its transverse components. The lower panel shows the averaged spatial distributions of accelerated electrons along the x direction at $\Omega_i t = 400.0$. The black solid, blue dotted, and red dashed curves represent the density of accelerated electrons averaged over the y and z directions with energy ranges 5-7 keV, 15-20 keV, and 60-200 keV, respectively. We find that electrons can be accelerated to relativistic energies at the quasi-parallel shock. The accelerated electrons concentrate close to the shock, indicating that electrons gain energy right at the shock front. At the end of the simulation, the maximum energy of the accelerated electrons has reached ~ 1 MeV. Those electrons have gyroradii large enough for them to resonantly interact with the injected magnetic fluctuations.

The strikingly efficient electron acceleration at a quasi-parallel shock has not been seen in previous numerical simulations (Guo & Giacalone 2010). As large-amplitude magnetic fluctuations convect across the shock, locally the shock can have a quasi-perpendicular geometry, which is expected to accelerate particles (Decker & Vlahos 1986; Giacalone 2005a). And, this occurs for long

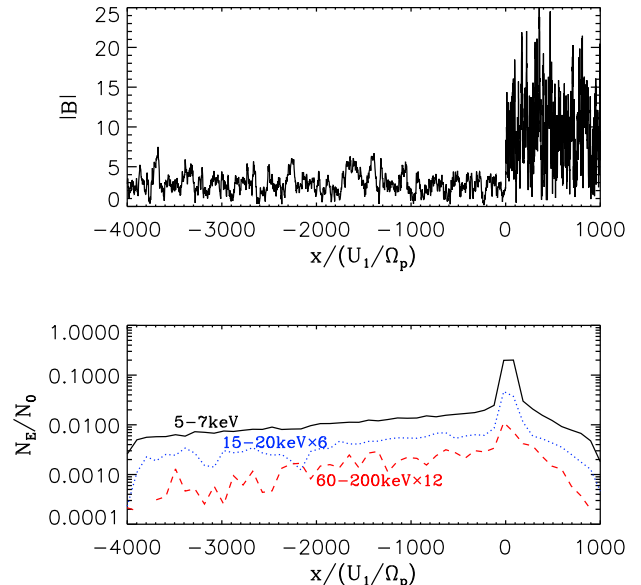


FIG. 1.— Upper panel: The magnitude of magnetic field across the shock wave. Lower panel: the averaged density of accelerated electrons in energy ranges 5-7 keV (black solid line), 15-20 keV (blue dotted line), and 60-200 keV (red dashed line).

enough of a time interval that the electrons gain significant energy. The effect of the magnetic variance of upstream fluctuations on electron acceleration at perpendicular shocks has been studied by Guo & Giacalone (2010, 2012a,b).

Figure 2 shows $\Gamma\%$, the fraction of accelerated electrons with $E > 10$ keV at the end of simulations as a function of θ_{Bn} for various wave variances $\sigma^2 = 0.1B_0^2$ (black solid line), $1.0B_0^2$ (blue dotted line), and $10.0B_0^2$ (red dashed line). The fraction for each run is also listed in Table 1. One can see that for the cases with $\sigma^2 = 0.1B_0^2$ and $1.0B_0^2$, the efficiency of electron acceleration is strongly dependent on the shock normal angle. However, for the case that $\sigma^2 = 10B_0^2$, the accelerated fraction varies from 7.3% for $\theta_{Bn} = 0^\circ$ to 11.4% for $\theta_{Bn} = 90^\circ$. This shows that the acceleration of electrons depends weakly on the shock angle when the wave variance in the upstream region is sufficiently large. Note that in this case, shocks with larger shock angles can still accelerate electrons more efficiently than shocks with smaller shock angles. It is also interesting to note that in the case with $\sigma^2 = B_0^2$ and $\theta_{Bn} = 90^\circ$ (Run 14), the fraction of electrons that reach 10 keV is higher than that in the case with larger turbulence variance $\sigma^2 = 10B_0^2$ and $\theta_{Bn} = 90^\circ$ (Run 21). This is because the local shock angles where particles interact with the shock is effectively reduced when stronger turbulence present in the shock region. For low energy particles, this effect makes more electrons accelerated to energies higher than 10 keV for the case with turbulence variance $\sigma^2 = B_0^2$.

Figure 3 shows the trajectory of a representative electron that is accelerated to more than $100E_0$ at a quasi-parallel shock with $\theta_{Bn} = 15^\circ$ and $\sigma^2 = 10B_0^2$ (Run 16). The upper panel displays the time evolution of the particle energy, the middle panel shows the position in the x direction, and the lower panel shows the energy as a function of position in the x direction between about $t = 300\Omega_i^{-1}$ (the injection time) and $t = 380\Omega_i^{-1}$,

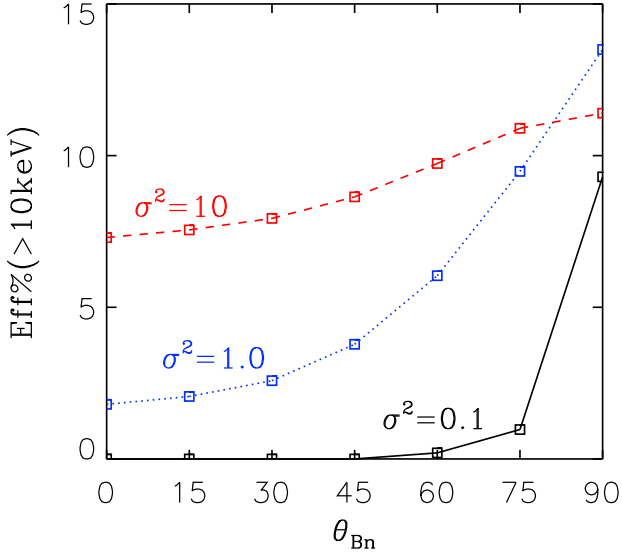


FIG. 2.— The efficiency of electron acceleration for various wave variances as a function of shock angle. $\Gamma\%$ is defined by the fraction of electrons that is accelerated to more than 10 keV at the end of the simulations.

respectively. The inset shows a blow-up close to the shock. The figure shows that the particle interacts with the shock numerous times and by which gains a large amount of energy. There are several large energy increases (e.g., during time period $t = 335\Omega_i^{-1} - 345\Omega_i^{-1}$) where the electron gains energy several times of its energy before the shock encounter. It also shows many small accelerations during which particles keep returning to the shock and obtaining multiple energy increases at the shock front. In the upstream region, the electron can also gain a small amount of energy as it gets reflected in the upstream medium. Recent publications have emphasized this process by using one-dimensional PIC simulations (Kato 2014; Park et al. 2014), but the shock speed is much larger $U_1 = 0.1 - 0.3c$ and the energy gain in each upstream reflection is $\Delta E \sim 2U_1 E/c$ in the downstream frame. For nonrelativistic shocks such as heliospheric shocks and supernova blast waves, this effect will be much reduced as we have shown here.

To better understand this, we closely examine the trajectory between $t = 300\Omega_i^{-1}$ (the injection time) and $t = 325\Omega_i^{-1}$. The upper two panels show the time evolutions of the particle's energy and position in the x direction respectively. During the time period 'a', the particle gains energy about 7 times of its energy before the shock encounter. In the middle panels, we closely examine the trajectory between $\Omega_i t = 306 - 310$, which is the time period marked by 'a' in the upper panels. The two plots show the time evolution of energy and the magnitude of magnetic field at the position of the electron. They clearly show that the electron gains energy while the magnetic field seen by the particle increases. This is typical of shock-drift acceleration. In the lower panels, we analyze the time period marked by 'b' in the upper panels. In this time duration, the electron has multiple shock encounters and each encounter corresponds to a small energy increase. Although we do not include fluctuations at scales associated with the gyroradii of the electrons at the injection energy which would cause pitch-

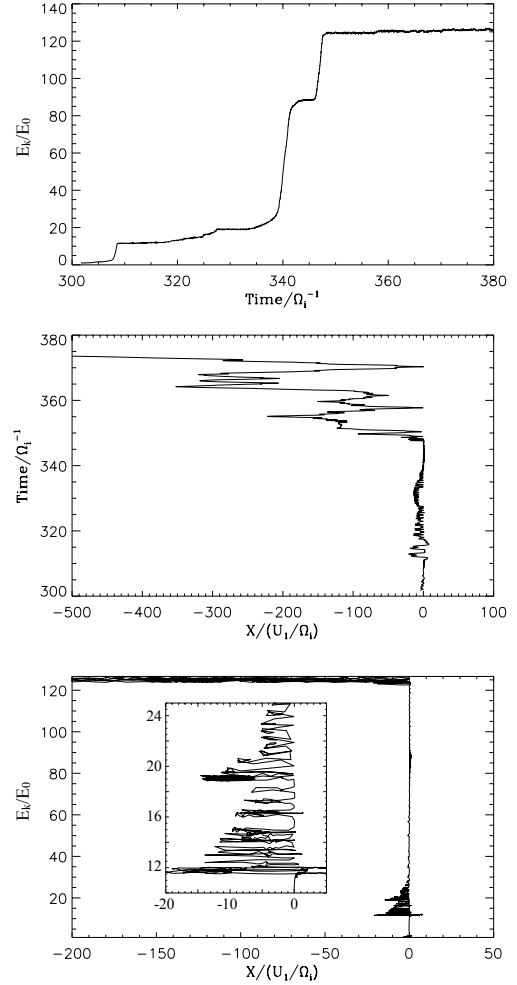


FIG. 3.— The trajectory analysis for an accelerated electron. The upper two panels show the evolution of energy and x position between $t = 120\Omega_i^{-1}$ and $t = 230\Omega_i^{-1}$. The middle panels show the time evolution of particle energy and the magnitude of magnetic field at the location of the electron during period 'a'. The bottom panels show similar quantities during period 'b'.

angle scattering, we find that electrons can be mirrored back to the shock when they encounter a sufficiently large magnetic field magnitude upstream of the shock. Note that when the electron is close to the shock, the typical spatial scale for the particle to get reflected immediately upstream is $\sim 20U_1/\Omega_i$, consistent with the scale of the upstream waves.

Figure 5 shows the downstream energy spectra of electrons at the end of simulation for a variety of runs. The black, blue, green and red solid lines are for $\sigma^2 = 10B_0^2$ with $\theta_{Bn} = 0^\circ$ (Run 15), 30° (Run 17), 60° (Run 19), and 90° (Run 21), respectively. For comparison, the spectra for $\sigma^2 = 0.1B_0^2$ with $\theta_{Bn} = 0^\circ$ (Run 1), and 90° (Run 7) are shown by the black dotted line and black dashed line, and the spectra for $\sigma^2 = B_0^2$ with $\theta_{Bn} = 0^\circ$ (Run 8), and 90° (Run 14) are shown by the blue dotted line and blue dashed line, respectively. One can see that when the wave variance of magnetic fluctuations is sufficiently large, the resulting energy spectrum does not significantly depend on the average shock-normal angle. In all the cases with $\sigma^2 = 10B_0^2$, electrons can be accelerated up to ~ 1 MeV. The spectra at quasi-parallel

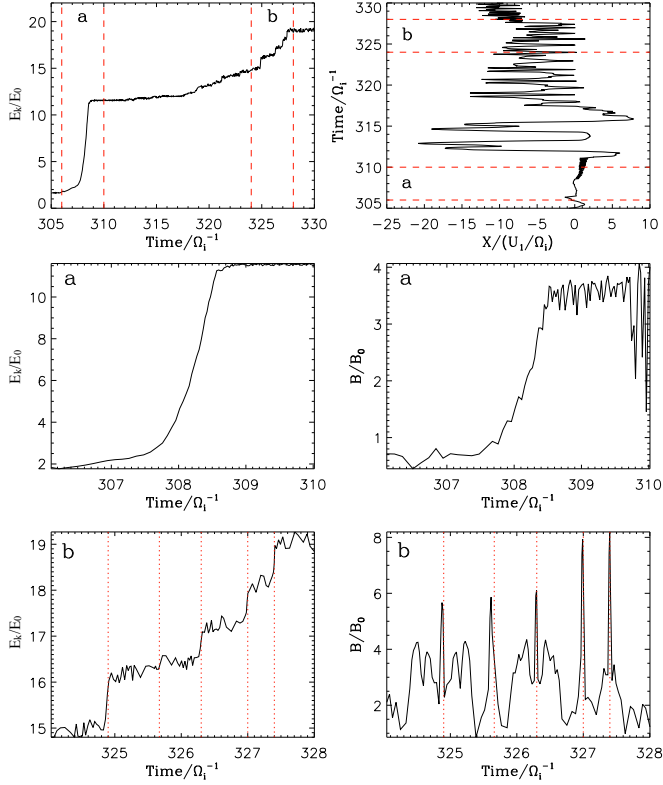


FIG. 4.— The trajectory analysis for an accelerated electron. The upper two panels show the evolution of energy and x position between $t = 120\Omega_i^{-1}$ and $t = 230\Omega_i^{-1}$. The middle panels show the time evolution of particle energy and the magnitude of magnetic field at the location of the electron during period ‘a’. The bottom panels show similar quantities during period ‘b’.

shocks are consistent with the recent observation of electron acceleration at a high-mach-number quasi-parallel shock associated with strong magnetic fluctuations (Masters et al. 2013). When the wave variance is $\sigma^2 = 0.1B_0^2$, perpendicular shocks can accelerate electrons more efficiently than parallel shocks and the resulting distributions depend strongly on the average shock normal angle. In this case the maximum electron energy can only reach 30 keV in the perpendicular shock case and 7 keV in the parallel shock case. When the wave variance is $\sigma^2 \geq B_0^2$, the energy spectra of accelerated electrons do not change much at perpendicular shocks, meaning the acceleration of electrons saturates when the wave variance is sufficiently large.

4. DISCUSSION AND CONCLUSIONS

In this paper, using numerical simulations, we calculated the trajectories of a large number of electrons encountering a shock that moves through a strongly fluctuating magnetic field. We found that the large-amplitude magnetic fluctuations have a significant effect on the acceleration of electrons. For the case that the wave variance $\sigma^2 \leq 1.0B_0^2$, the acceleration of electrons strongly depends on the average shock normal angle. However, in the case that $\sigma^2 \sim 10B_0^2$, electrons can be accelerated efficiently to relativistic energies regardless of the shock angle. This indicates that the acceleration of electrons is weakly dependent on the average shock normal angle when the upstream wave variance is sufficiently large.

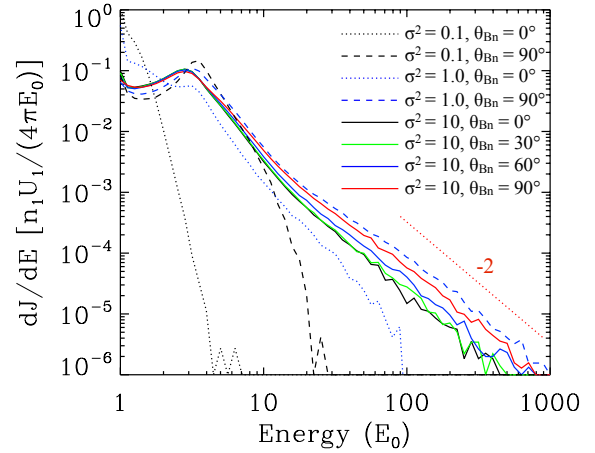


FIG. 5.— Energy spectra of electrons in the downstream region at the end of simulation for a variety of runs. The black, blue, green and red solid lines are for $\sigma^2 = 10B_0^2$ with $\theta_{Bn} = 0^\circ$ (Run 15), 30° (Run 17), 60° (Run 19), and 90° (Run 21), respectively. For comparison, the spectra for $\sigma^2 = 0.1B_0^2$ with $\theta_{Bn} = 0^\circ$ (Run 1), and 90° (Run 7) are shown by the black dotted line and black dashed line, and the spectra for $\sigma^2 = B_0^2$ with $\theta_{Bn} = 0^\circ$ (Run 8), and 90° (Run 14) are shown by the black dotted line and black dashed line, respectively.

This is also consistent with recent observation by Masters et al. (2013), who reported *in situ* measurements showing that electrons get accelerated to relativistic energies at a high-mach-number quasi-parallel shock that is associated with strong magnetic fluctuations with $\delta B/B_0 \sim 10$ or larger. We find electrons can be reflected by strong magnetic field in the upstream region and get accelerated at the shock though drift acceleration. The energy spectra of electrons in the end of the simulation for different shock angles are remarkably similar, indicating that they are accelerated by the same process. In our simulation, electrons are accelerated up to $\sim 1\text{ MeV}$ within several hundred proton gyroperiods. At that energy the accelerated electrons have gyroradii large enough to resonantly interact with the injected magnetic fluctuations. This provides an efficient mechanism for injecting electrons into diffusive shock acceleration and is important to explain electron acceleration and high-energy emissions at astrophysical shocks (Kang et al. 2012).

Finally, we note that although this study shows that the acceleration of electrons can be efficient at quasi-parallel shocks when there exists large-amplitude magnetic fluctuations, which is consistent with the observation made by Masters et al. (2013), the origin of the strong magnetic fluctuations is not clear. Large-amplitude magnetic fluctuations have been inferred to be present in the vicinity of high-Mach-number supernova shocks (Berezhko et al. 2003). However, the dominate mechanism is still under debate (Bell 2004; Giacalone & Jokipii 2007; Amato & Blasi 2009; Inoue et al. 2009; Guo et al. 2012; Greenfield et al. 2012). The Masters et al. (2013) observation shows that ions are only accelerated to $\sim 10\text{ keV}$, indicating in this case the effect of energetic protons on generating strong magnetic fluctuations is not significant. Studying the generation of large-amplitude magnetic fluctuations is beyond the scope of the present study and we will revisit this problem in future work.

ACKNOWLEDGEMENT

F.G. benefited from discussion with Dr. Hongqing He and Dr. Yi-Hsin Liu. This work was supported by NASA under grant NNX11AO64G and by NSF under

grant AGS1154223 and AGS1135432. Part of the computational resource supporting this work were provided by the institutional computing resources at Los Alamos National Laboratory.

REFERENCES

- Amano, T., & Hoshino, M. 2007, *ApJ*, 661, 190
 —. 2010, *Physical Review Letters*, 104, 181102
 Amato, E., & Blasi, P. 2009, *MNRAS*, 392, 1591
 Anderson, K. A., Lin, R. P., Martel, F., Lin, C. S., Parks, G. K., & Reme, H. 1979, *Geophys. Res. Lett.*, 6, 401
 Axford, W. I., Leer, E., & Skadron, G. 1977, in *Proc. 15th Int. Cosmic-Ray Conf. (Plovdiv)*, Vol. 11, , 273
 Bale, S. D., Mozer, F. S., & Horbury, T. S. 2003, *Physical Review Letters*, 91, 265004
 Ball, L., & Melrose, D. B. 2001, *PASA*, 18, 361
 Batchelor, G. K. 1953, *The Theory of Homogeneous Turbulence*, Cambridge: Cambridge University Press, 1953
 Bell, A. R. 1978, *MNRAS*, 182, 147
 —. 2004, *MNRAS*, 353, 550
 Berezhko, E. G., Ksenofontov, L. T., & Völk, H. J. 2003, *A&A*, 412, L11
 Blandford, R., & Eichler, D. 1987, *Phys. Rep.*, 154, 1
 Blandford, R. D., & Ostriker, J. P. 1978, *ApJ*, 221, L29
 Burgess, D. 2006, *ApJ*, 653, 316
 Caprioli, D., & Spitkovsky, A. 2013, *ApJ*, 765, L20
 Cliver, E. W. 2009, in *IAU Symposium*, Vol. 257, *Universal Heliophysical Processes*, ed. N. Gopalswamy & D. F. Webb (London: Cambridge Univ. Press), 401–412
 Decker, R. B. 1988, *Space Sci. Rev.*, 48, 195
 Decker, R. B., Krimigis, S. M., Roelof, E. C., Hill, M. E., Armstrong, T. P., Gloeckler, G., Hamilton, D. C., & Lanzerotti, L. J. 2005, *Science*, 309, 2020
 Decker, R. B., & Vlahos, L. 1986, *ApJ*, 306, 710
 Eriksen, K. A., et al. 2011, *ApJ*, 728, L28
 Fan, C. Y., Gloeckler, G., & Simpson, J. A. 1964, *Physical Review Letters*, 13, 149
 Feng, S. W., Chen, Y., Kong, X. L., Li, G., Song, H. Q., Feng, X. S., & Guo, F. 2013, *ApJ*, 767, 29
 Feng, S. W., Chen, Y., Kong, X. L., Li, G., Song, H. Q., Feng, X. S., & Liu, Y. 2012, *ApJ*, 753, 21
 Giacalone, J. 2005a, *ApJ*, 624, 765
 —. 2005b, *ApJ*, 628, L37
 Giacalone, J., & Ellison, D. C. 2000, *J. Geophys. Res.*, 105, 12541
 Giacalone, J., & Jokipii, J. R. 1994, *ApJ*, 430, L137
 —. 1996, *J. Geophys. Res.*, 101, 11095
 —. 1999, *ApJ*, 520, 204
 —. 2007, *ApJ*, 663, L41
 —. 2009, *ApJ*, 701, 1865
 Gosling, J. T., Thomsen, M. F., Bame, S. J., & Russell, C. T. 1989, *J. Geophys. Res.*, 94, 10011
 Greenfield, E. J., Jokipii, J. R., & Giacalone, J. 2012, *ArXiv e-prints* 1205.0269
 Guo, F., & Giacalone, J. 2010, *ApJ*, 715, 406
 —. 2012a, *ApJ*, 753, 28
 Guo, F., & Giacalone, J. 2012b, in *American Institute of Physics Conference Series*, Vol. 1500, *American Institute of Physics Conference Series*, ed. Q. Hu, G. Li, G. P. Zank, X. Ao, O. Verkhoglyadova, & J. H. Adams, 93–99
 —. 2013, *ApJ*, 773, 158
 Guo, F., Li, S., Li, H., Giacalone, J., Jokipii, J. R., & Li, D. 2012, *ApJ*, 747, 98
 Haggerty, D. K., & Roelof, E. C. 2009, in *American Institute of Physics Conference Series*, Vol. 1183, *American Institute of Physics Conference Series*, ed. X. Ao & G. Z. R. Burrows, 3–10
 Hellinger, P., Trávníček, P., Lembège, B., & Savoini, P. 2007, *Geophys. Res. Lett.*, 34, 14109
 Hoshino, M., & Shimada, N. 2002, *ApJ*, 572, 880
 Inoue, T., Yamazaki, R., & Inutsuka, S.-i. 2009, *ApJ*, 695, 825
 Jokipii, J. R. 1982, *ApJ*, 255, 716
 —. 1987, *ApJ*, 313, 842
 Jokipii, J. R., & Giacalone, J. 2007, *ApJ*, 660, 336
 Jokipii, J. R., Kota, J., & Giacalone, J. 1993, *Geophys. Res. Lett.*, 20, 1759
 Jones, F. C., Jokipii, J. R., & Baring, M. G. 1998, *ApJ*, 509, 238
 Kang, H., Ryu, D., & Jones, T. W. 2012, *ApJ*, 756, 97
 Kato, T. N. 2014, *ArXiv e-prints*
 Kato, T. N., & Takabe, H. 2010, *ApJ*, 721, 828
 Kozarev, K. A., Korreck, K. E., Lobzin, V. V., Weber, M. A., & Schwadron, N. A. 2011, *ApJ*, 733, L25
 Krasnoselskikh, V. V., Lembège, B., Savoini, P., & Lobzin, V. V. 2002, *Physics of Plasmas*, 9, 1192
 Krauss-Varban, D., Burgess, D., & Wu, C. S. 1989, *J. Geophys. Res.*, 94, 15089
 Krymsky, G. F. 1977, *Akademiia Nauk SSSR Doklady*, 234, 1306
 Levinson, A. 1992, *ApJ*, 401, 73
 —. 1994, *ApJ*, 426, 327
 Masters, A., et al. 2013, *Nature Physics*, 9, 164
 Matsukiyo, S., & Scholer, M. 2006, *Journal of Geophysical Research (Space Physics)*, 111, 6104
 Niemiec, J., Pohl, M., Bret, A., & Wieland, V. 2012, *ApJ*, 759, 73
 Oka, M., et al. 2006, *Geophys. Res. Lett.*, 332, L24104
 Park, J., Caprioli, D., & Spitkovsky, A. 2014, *ArXiv e-prints*
 Park, J., Workman, J. C., Blackman, E. G., Ren, C., & Siller, R. 2012, *Physics of Plasmas*, 19, 062904
 Press, W. H., Flannery, B. P., & Teukolsky, S. A. 1986, *Numerical recipes. The art of scientific computing*, ed. Press, W. H., Flannery, B. P., & Teukolsky, S. A.
 Reynolds, S. P. 2008, *ARA&A*, 46, 89
 Riquelme, M. A., & Spitkovsky, A. 2011, *ApJ*, 733, 63
 Shimada, N., & Hoshino, M. 2000, *ApJ*, 543, L67
 Shimada, N., Terasawa, T., Hoshino, M., Naito, T., Matsui, H., Koi, T., & Maezawa, K. 1999, *Ap&SS*, 264, 481
 Simnett, G. M., Sakai, J., & Forsyth, R. J. 2005, *A&A*, 440, 759
 Umeda, T., Yamao, M., & Yamazaki, R. 2009, *ApJ*, 695, 574
 Wilson, III, L. B., et al. 2012, *Geophys. Res. Lett.*, 39, 8109
 Wu, C. S. 1984, *J. Geophys. Res.*, 89, 8857
 Wu, C. S., Winske, D., Papadopoulos, K., Zhou, Y. M., Tsai, S. T., & Guo, S. C. 1983, *Physics of Fluids*, 26, 1259
 Yang, Z. W., Lembège, B., & Lu, Q. M. 2012, *Journal of Geophysical Research (Space Physics)*, 117, 7222
 Yuan, X., Cairns, I. H., & Robinson, P. A. 2008, *Journal of Geophysical Research (Space Physics)*, 113, A08109